Chemical Geology 255 (2008) 134–142

Contents lists available at ScienceDirect

Chemical Geology

journal homepage: www.elsevier.com/locate/chemgeo

U–Th systematics of dispersed young volcanoes in NE China: Asthenosphere upwelling caused by piling up and upward thickening of stagnant Pacific slab

Haibo Zou [a,*], Qicheng Fan [b], Yupeng Yao [c]

[a] Department of Earth and Space Sciences and Institute of Geophysics and Planetary Physics, University of California, Los Angeles, CA 90095, USA
[b] Institute of Geology, China Earthquake Administration, Beijing 100029, China
[c] Institute of Geology and Geophysics, Chinese Academy of Sciences, Beijing 100029, China

ARTICLE INFO

Article history:
Received 14 September 2007
Received in revised form 8 June 2008
Accepted 14 June 2008

Editor: B. Bourdon

Keywords:
Basalts
Pacific slab
U–Th disequilibrium
Melt generation
Magma residence time

ABSTRACT

Young (300 to 5500years old) dispersed intraplate volcanism characterized by small volume of melt and large compositional variability, occurred over NE China at Jingbohu, Long-gang, Tianchi and Wudalianchi. These young volcanic rocks provide ideal opportunities for investigating the mechanism of dispersed continental volcanism using short-lived uranium-series isotopes. We present systematic U-series, Nd, Sr, Pb isotope and trace element analyses of the young lavas from NE China. Jingbohu lavas display variable extents of ^{230}Th excesses (10 to 28%) and moderately depleted Nd isotopic compositions (ε_{Nd} = + 1.5 to + 3.3). Long-gang lavas have pronounced (33 to 35%) ^{230}Th excesses and slightly depleted Nd isotopic compositions (ε_{Nd} = + 0.5 to + 0.7). The Tianchi lavas display moderate (12%) ^{230}Th excesses and slightly enriched Nd isotopic compositions (ε_{Nd} = − 1.0 to − 1.1). ^{230}Th enrichments in all these volcanic rocks are uncharacteristic of melts generated by subduction. The strongest evidence against the involvement of subduction-related fluids is derived from the Long-gang lavas having more than 30% ^{230}Th excesses, low U/Th, Sr/Th and Ba/Th ratios, and positive Nb and Ta anomalies. The fluids released from the subduction of the Pacific plate under the Eurasian plate might have already been completely lost before the slab reached the mantle beneath NE China. We postulate that, in addition to the convective circulation process, the continuous piling up and upward thickening of stagnant Pacific slab in the mantle transition zone may help drive a broad asthenosphere upwelling far from the trench, leading to mantle partial melting and the formation of the young volcanoes in NE China. In addition, our U–Th disequilibrium data provide constraints on magma evolution time. The magma evolution time from low SiO_2 (47.5%) basalt to higher SiO_2 (50.4%) basalt at Long-gang is within 10 thousand years (10ka). The magma evolution time from trachyte to rhyolite at Tianchi volcano is also less than 10ka. If the Tianchi silicic rocks were evolved from Long-gang basaltic magmas with minor crustal assimilation, then the magma evolution time from basaltic magma to silicic magmas is less than 110 thousand years.

1. Introduction

Dispersed Cenozoic lavas are widely distributed in East Asia and constitute a diffuse igneous province (e.g., Basu et al., 1991; Flower et al., 1998; Zou et al., 2000; Choi et al., 2006). Such provinces differ from large igneous provinces that were generated from mantle plume melting by having greater compositional diversity and lower rates of melt production (Flower et al., 1998; Farmer, 2004). In comparison with the understanding of the formation of flood basalts from large igneous provinces, how small-volume dispersed continental lavas are generated is not well understood. Why and where did the melting occur that eventually led to the formation of such small-volume dispersed lavas on continent?

Northeast China is an ideal place to study dispersed continental volcanism using short-lived uranium-series isotopes, owing to the presence of diverse small-volume Holocene (< 10,000) lavas at Wudalianchi, Jingbohu, Long-gang, and Tianchi (the youngest volcano at Changbaishan or Baitoushan). The eruption ages are 1719–1721 AD for Wudalianchi, 5200–5500years BP (before present) for Jingbohu (Fan et al., 2003; Fan et al., 2006), 1500–1600years BP for Long-gang (Fan et al., 2002), and about 1000years BP for Tianchi (Dunlap et al., 1992; Horn and Schmincke, 2000; Wei et al., 2007). Lavas from Jingbohu and Long-gang contain mantle xenoliths, indicating fast magma transport to the surface.

A U-series study of the Wudalianchi potassic basalts has already been conducted (Zou et al., 2003). Here we carry out a systematic U–Th disequilibrium, Nd, Sr and Pb isotope as well as major and trace element study of the Holocene lavas from Jingbohu, Long-gang and Tianchi of NE China, in order to 1) investigate the origins of the Holocene lavas in a diffuse igneous province; 2) assess possible

* Corresponding author. Present Address: Department of Geology and Geography, Auburn University, Auburn, AL 36849, USA. Tel.: +1 334 844 4315; fax: +1 334 844 4486.
E-mail address: haibo.zou@auburn.edu (H. Zou).

0009-2541/$ – see front matter © 2008 Elsevier B.V. All rights reserved.
doi:10.1016/j.chemgeo.2008.06.022

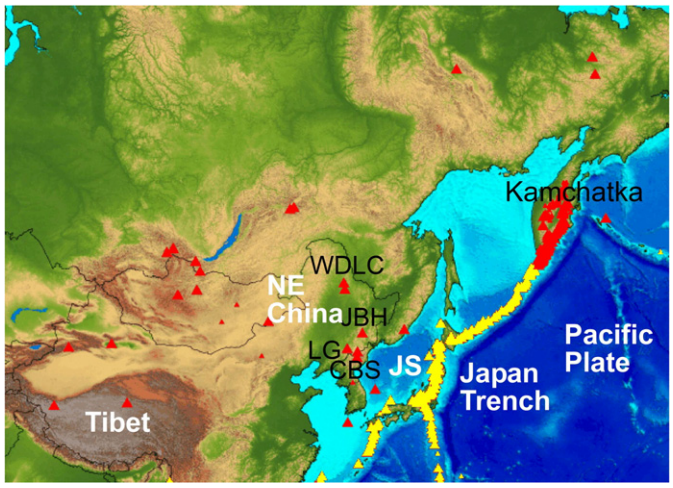

Fig. 1. Locations of Holocene volcanoes in NE China. WDLC = Wudalianchi; JBH = Jingbohu; LG = Long-gang; CBS = Changbaishan (Baitoushan). Tianchi volcano is the youngest volcano at Changbaishan.

influence of recent subduction-related fluids beneath NE China; and 3) constrain the magma evolution time scales for evolved lavas from Tianchi (Fig. 1).

2. Analytical methods

Thorium isotopic compositions of most samples were measured using a VG 54 mass spectrometer equipped with a WARP energy filter (VG54-WARP) and an ion counting system, except for three samples (J99821-1, J99824-1 and JB11-11) that were measured by a Cameca IMS 1270 ion microprobe at UCLA, following Layne and Sims (2000). The mass resolution for the ion probe IMS 1270 work is at 5000. In principle, the ion probe technique for Th isotope measurement is similar to the ISOLAB 54 secondary ion mass spectrometry technique originally developed at Lamont (England et al., 1992; Bourdon, 1994).

The revised chemical method at UCLA to separate and purify thorium involves two columns (1) a 400 μl TRU Spec column to separate Th from other major and trace elements, and (2) a 100 μl anion resin column to purify Th. Chemically separated high-purity Th was loaded inside a circular containment in a 1-inch diameter graphite disk. Repeated analyses for Th isotopic standards are $^{232}Th/^{230}Th$ = 1.703×10^5 10^5 ± 1.5×10^3 (n = 37) (2 SD) for UC Santa Cruz Th standard TML-1, which is in accord to the working value of 1.706×10^5 ± 1.4×10^3 (Collerson et al., 1997; Layne and Sims, 2000). Analyses of a thorium solution standard (WUN-1) give $^{232}Th/^{230}Th = 2.303\times10^5 \pm 2.5\times10^3$ (n = 6), within error of the analyses obtained using ISOLAB 54 at the National High Magnetic Field Laboratory ($2.327\times10^5 \pm 2.4\times10^3$) (Zou et al., 2002; Stracke et al., 2003), Cameca IMS 1270 at Woods Hole ($2.305\times10^5 \pm 2.3\times10^3$), Finnigan Neptune at Woods Hole ($2.336\times10^5 \pm 1.5\times10^3$) (Ball et al., 2002) and VG Elemental Plasma 54-30 ($2.316\times10^5 \pm 0.7\times10^3$) at Carnegie Institution of

Table 1
Major element (in wt.%) and trace element (ppm) concentrations of lavas from Jingbohu (JBH), Long-gang (LG) and Tianchi (TC)

Sample	J99821-1	J99821-5	J99821-6	J99822-1	J99823-1	J99824-1	JB11-11	LG 9940	99L11-1	HJ97001A	HJ97034	HJ97044	P-2	P-4
Locality	JBH	JBH	JBH	JBH	JBH	JBH	JBH	LG	LG	LG	LG	LG	TC	TC
SiO_2	47.43	47.84	44.97	50.08	51.08	46.39	46.78	47.45	50.38	49.76	48.50	48.51	71.63	64.04
TiO_2	1.69	1.71	1.83	1.79	2.25	1.77	1.92	2.52	1.89	1.94	2.39	2.31	0.23	0.57
Al_2O_3	15.13	15.08	14.98	16.92	13.57	14.87	17.06	16.38	17.69	17.70	16.52	17.03	11.27	15.69
Fe_2O_3*	11.76	10.54	11.55	9.95	9.01	10.42	11.36	11.53	11.47	11.60	11.51	11.42	4.15	5.13
MnO	0.17	0.17	0.17	0.14	0.13	0.17	0.15	0.17	0.26	0.18	0.19	0.20	0.05	0.10
MgO	8.04	8.13	8.5	4.39	7.31	9.03	4.67	7.43	4.60	4.46	6.74	5.65	0.36	1.58
CaO	8.46	7.96	8.41	5.64	7.12	8.30	5.77	7.65	6.00	5.76	8.01	7.82	0.04	0.42
Na_2O	4.47	4.92	4.96	6.09	3.78	4.77	6.20	3.97	3.72	4.25	3.42	3.76	4.81	5.68
K_2O	2.32	2.88	3.27	4.07	4.50	3.00	4.59	2.31	3.06	3.01	2.29	2.05	5.39	5.56
P_2O_5	0.72	0.91	0.96	1.03	0.93	0.99	1.06	0.57	0.00	0.88	0.53	0.67	0.00	0.10
Total	100.19	100.13	99.6	100.10	99.67	99.71	99.56	99.99	99.07	99.54	100.09	99.43	99.53	99.59
Cs	0.79	0.97	0.69	1.25	0.89	0.87	1.22	0.70	2.00	0.57	0.60	0.82	5.76	2.66
Rb	51.4	57.7	42.5	85.9	58.1	56.5	82.2	56.0	82.9	55.9	55.4	89.7	297.0	116.0
Ba	652	636	668	697	678	680	689	806	1192	778	782	968	15.3	148
Th	8.13	8.59	7.84	11.41	7.83	8.47	11.22	6.67	9.99	6.69	7.26	10.70	46.93	14.26
U	1.98	2.15	1.64	2.85	1.85	2.18	2.71	1.31	1.94	1.35	1.44	1.52	9.79	2.72
Nb	73.1	68.9	62.6	89.2	82.4	76.5	93.8	58.7	76.3	56.5	58.4	72.8	201.3	68.1
Ta	4.21	4.00	3.57	5.66	4.99	4.43	5.75	3.49	4.60	3.41	3.87	5.57	16.33	5.37
La	59.2	56.5	47.1	65.2	66.8	62.5	67.3	46.2	68.6	45.5	45.7	58.7	135.0	67.2
Ce	106.1	101.9	83.7	118.7	112.6	111.6	123.0	84.9	122.4	83.6	88.8	109.5	301.4	138.9
Pb	5.15	7.02	4.80	10.00	6.30	5.91	7.31	4.39	6.59	4.79	5.89	7.69	37.14	14.67
Pr	11.9	11.4	9.3	13.3	12.4	12.5	13.8	9.50	13.15	9.32	9.64	11.7	34.4	16.0
Sr	1011	960	759	1047	1075	1066	1136	795	955	711	693	802	6.85	56.15
Nd	45.4	43.3	35.3	50.4	46.7	47.8	52.5	35.8	47.5	35.3	33.1	39.2	113.6	56.3
Zr	246	239	199	355	259	254	385	208	286	213	209	265	1724	560
Hf	5.55	5.52	4.63	8.04	5.39	5.57	8.46	5.12	6.46	5.18	5.72	7.08	48.00	14.48
Sm	8.92	8.46	7.18	9.61	9.12	9.38	10.11	7.09	8.53	6.99	6.54	7.64	25.40	10.90
Eu	2.87	2.69	2.43	2.98	2.71	2.99	3.24	2.42	2.85	2.39	2.35	2.80	0.32	0.74
Gd	7.58	7.44	6.47	7.76	7.68	8.35	8.09	6.25	7.18	6.29	7.01	6.92	25.70	10.00
Tb	1.11	1.06	0.94	1.03	1.03	1.14	1.07	0.94	1.05	0.94	0.94	0.97	4.11	1.56
Dy	5.75	5.64	5.13	5.19	5.24	6.06	5.21	5.29	5.94	5.22	4.53	4.57	21.44	7.56
Ho	1.01	1.00	0.92	0.82	0.90	1.03	0.81	0.97	1.10	0.97	0.83	0.89	4.27	1.47
Er	2.36	2.38	2.21	1.72	2.18	2.37	1.66	2.42	2.92	2.46	2.18	2.15	11.20	3.63
Yb	1.64	1.68	1.60	1.07	1.57	1.56	0.87	1.94	2.54	1.90	2.11	1.70	9.73	3.42
Y	25.2	25.0	23.0	20.5	27.5	25.8	20.1	23.8	28.3	24.3	22.4	21.6	96.7	29.4
Lu	0.23	0.25	0.24	0.15	0.23	0.23	0.11	0.29	0.39	0.29	0.38	0.31	1.36	0.49
Eu*	1.04	1.01	1.07	1.02	0.97	1.01	1.06	1.09	1.08	1.08	1.05	1.15	0.04	0.21
Sr/Th	124	112	97	92	137	126	101	119	96	106	95	75	0.1	3.9
Ba/Th	80	74	85	61	87	80	61	121	119	116	108	90	0.33	10

Eu anomaly is given by $Eu^* = 2Eu_N/(Sm_N + Gd_N)$, where N denotes normalized values by CI chondrite.

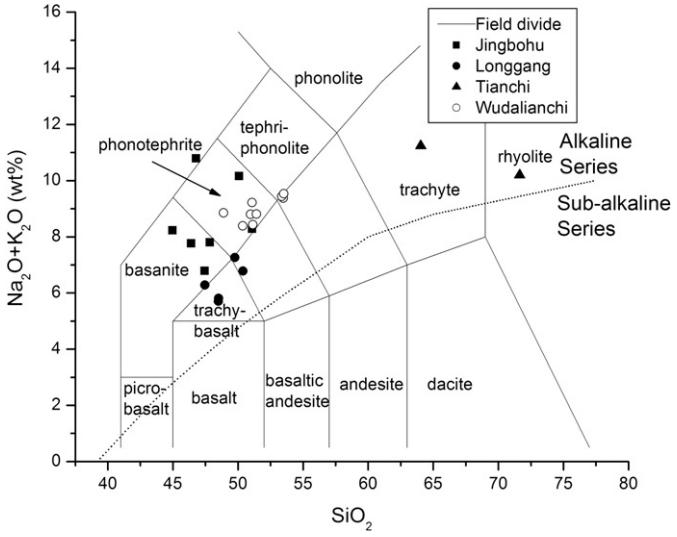

Fig. 2. Total alkali vs. silica (TAS) plot. The classification is based on Le Bas et al. (1986). The dotted line is the division between alkaline series and subalkaline series (Irvine and Baragar, 1971).

Washington (Pietruszka et al., 2002). Reproducibility of $^{238}U/^{232}Th$ ratios is estimated to be < 1.5%, based on isotope dilution analyses of U/Th ratios of TML-1 from 3 separate dissolutions.

Major and trace elements were measured by ICP-MS at the GeoAnalytical Center at the Washington State University and the Institute of Geology and Geochemistry, Chinese Academy of Sciences. Sample powders were prepared with an agate mill to avoid potential contamination of Ta and Nb by a tungsten carbide mill. Nd, Sr and Pb isotopic compositions as well as U and Th concentrations were measured using VG 54 WARP at UCLA. Analytical details on Nd, Sr and Pb isotopes and U and Th concentrations at UCLA using TIMS have been documented in Zou et al. (2003). Nd and Sr isotopic compositions were normalized to $^{146}Nd/^{144}Nd = 0.7219$ and $^{86}Sr/^{88}Sr = 0.1194$, respectively. The measured Nd and Sr isotope standard values are $^{143}Nd/^{144}Nd = 0.511843 \pm 13$ ($n = 24$) for La Jolla and $^{87}Sr/^{86}Sr = 0.710239 \pm 16$ ($n = 13$) for NBS 987. Replicate analyses of Pb isotope standard NBS 981 give $^{206}Pb/^{204}Pb = 16.896 \pm 0.013$, $^{207}Pb/^{204}Pb = 15.435 \pm 0.014$, and $^{208}Pb/^{204}Pb = 36.525 \pm 0.041$. Relative to the following values for NBS981: $^{206}Pb/^{204}Pb = 16.9356$, $^{207}Pb/^{204}Pb = 15.4891$, and $^{208}Pb/^{204}Pb = 36.7006$ (Todt et al., 1996), Pb isotopic data in samples were corrected for mass fractionation of 0.118% per atomic mass unit (AMU) for $^{206}Pb/^{204}Pb$, 0.117% per AMU for $^{207}Pb/^{204}Pb$, and 0.119% per AMU for $^{208}Pb/^{204}Pb$.

3. Results

We selected 14 samples for major and trace element analyses, including 7 samples from Jingbohu, 5 samples from Long-gang and 2 samples from Tianchi. Major and trace element concentrations (in wt.%) are presented in Table 1. In the total alkali vs. silica (TAS) diagram, all samples belong to the alkaline series (above the dotted line in Fig. 2). The 12 samples from Jingbohu and Long-gang are alkali basalts and the 2 samples from Tianchi are trachyte (P-4) and rhyolite (P-2). In detail, the 7 samples from Jingbohu are basanite and phototephrite, and the 5 samples from Long-gang are trachybasalts. The alkali basalts from Jingbohu and Long-gang have similar SiO_2 content (47–50%). The MgO content varies from 9.0% to 4.4% for Jingbohu, and from 7.4% to 4.5% for Long-gang. The total alkali contents range from 6.8% to 10.8% for Jingbohu, and from 5.7% to 7.2% for Long-gang. Except for sample J99823-1, the alkali basalts have $K_2O/Na_2O < 1.0$. The alkali basalts from Jingbohu and Long-gang have high TiO_2 contents, ranging from 1.7 to 2.4%.

All alkali basalts from Jingbohu and Long-gang are enriched in light rare earth elements (LREEs) over heavy rare earth elements (HREEs) (Fig. 3). They do not display any negative Eu anomalies. In the spider diagram (Fig. 4), none of the samples shows any appreciable depletion in high field strength elements, such as Nb and Ta.

The evolved lavas from Tianchi are also enriched in LREE over HREE. The Tianchi lavas have significant negative Eu anomalies ((Eu*) 0.04 is for rhyolitic sample P-2 and 0.21 for trachytic sample P-4), suggesting considerable plagioclase fractionation. The Tianchi trachyte (P-4) and especially rhyolite (P-2) display strong negative anomalies in Ba, Sr, and Ti (Fig. 4).

The Nd, Sr, Pb and U-series isotope data are presented in Table 2. The Sr, Nd and Pb isotope data show highly restricted range within each locality. The ε_{Nd} values are + 1.5 to + 3.2 for Jingbohu, + 0.5 to + 0.7 for Long-gang, and − 1.0 to − 1.1 for Tianchi. The $^{87}Sr/^{86}Sr$ values range from 0.7039 to 0.7044 for Jingbohu, 0.7044 to 0.7045 for Long-gang, and 0.7050 to 0.7052 for Tianchi. The $^{206}Pb/^{204}Pb$ ratios are 17.88 to 18.00 for Jingbohu, 17.91 to 17.95 for Long-gang, and 17.54 to 17.56 for Tianchi. Samples from Jingbohu, Long-gang and Tianchi display higher ε_{Nd} and $^{206}Pb/^{204}Pb$, but lower $^{87}Sr/^{86}Sr$ than Wudalianchi potassic basalts (Fig. 5). The Nd isotope compositions indicate that source rocks for the Jingbohu and Long-gang lavas are moderately depleted and may represent asthenospheric melts. The slightly negative ε_{Nd} value

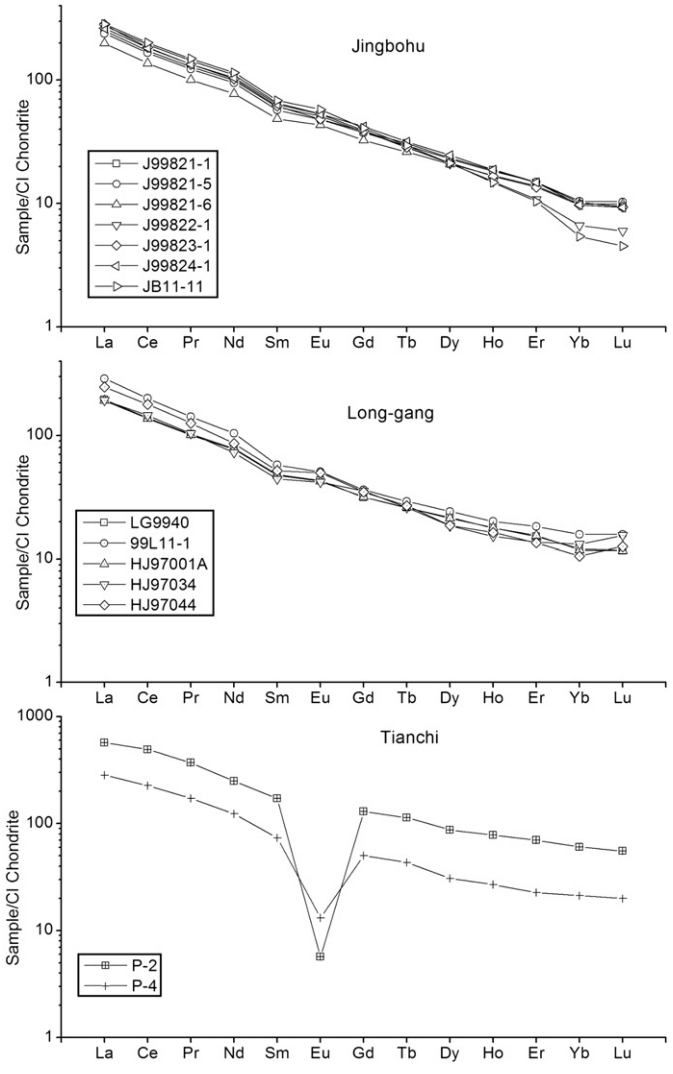

Fig. 3. CI chondrite-normalized REE abundance patterns for the lavas from (a) Jingbohu, (b) Long-gang and (c) Tianchi.

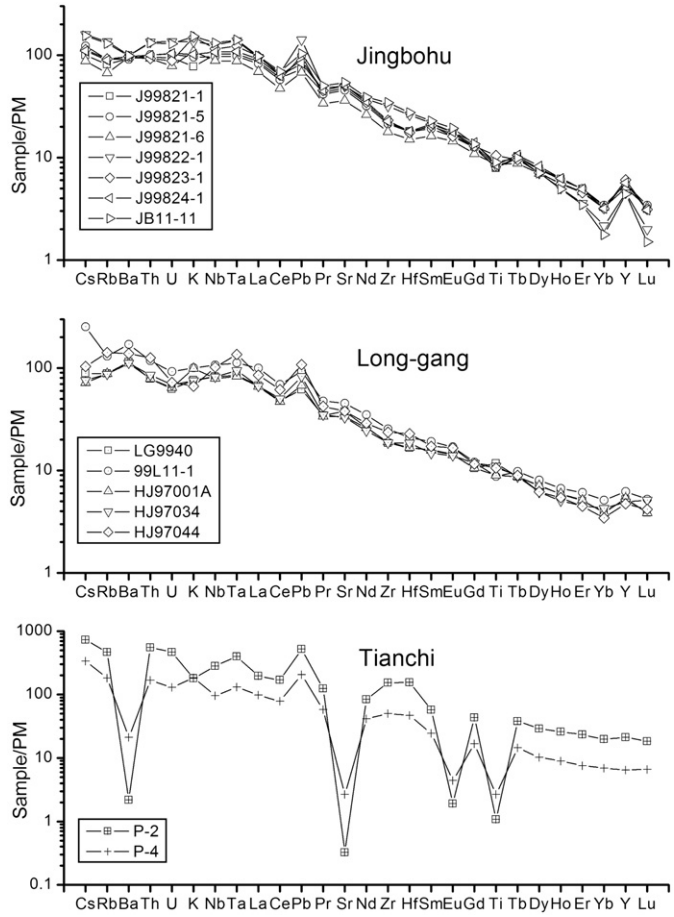

Fig. 4. Primitive mantle (Sun and McDonough, 1989) normalized spider trace element diagrams for lavas from (a) Jingbohu, (b) Long-gang, and (c) Tianchi.

of the Tianchi evolved lavas may be attributed to minor crustal assimilation during fractional crystallization process.

The U–Th isotope results are presented on a (^{230}Th/^{232}Th) vs. (^{238}U/^{232}Th) equiline diagram in Fig. 6. All samples, in particular, the Long-gang samples, display significant ^{230}Th excesses (Fig. 6). The (^{230}Th/^{238}U) values are 1.09 to 1.28 for Jingbohu, 1.33 to 1.35 for Long-gang, and 1.12 for Tianchi. Interestingly, the three samples (LG9940, 99L11-1, HJ97001A) from Long-gang exhibit (^{230}Th/^{238}U) ratios (1.33 to 1.35) within measurement uncertainties, in spite of their MgO range (7.43%, 4.60% and 4.46%, respectively). The two Tianchi samples (P-2 and P-4) have identical (^{230}Th/^{238}U) value (1.12), despite their differences in MgO content (1.6% for P-4 and 0.4% for P-2) and SiO_2 content (64% for P-4 and 71.6% for P-2). The (^{230}Th/^{238}U) values are not correlated to ε_{Nd} values. For example, the Long-gang lavas have the highest (^{230}Th/^{238}U) (1.33 to 1.35) but only the intermediate ε_{Nd} value (+0.5 to +0.7).

The Holocene basalts from western USA are also plotted in Fig. 6 for reference purposes. In general, the NE China basalts have higher ^{230}Th excesses and lower U/Th ratios than the western USA basalts.

4. Discussion

4.1. Assessment of the influence of fluids released from subducted Pacific slab

A fundamental question regarding the geodynamics in NE China is whether or not the dispersed volcanoes are physically and chemically associated with the subduction of the Pacific plate. Recent study of seismic topography indicates that the Pacific plate subducts from Japan trench and gradually flattens at a depth of 400 to 600 km (in the transition zone) in the NE China volcanic region (Zhao, 2004; Lei and Zhao, 2005). The stagnant slab may carry fluids deep into the mantle (Zhao, 2004; Lei and Zhao, 2005). It was proposed that the deep dehydration process of the stagnant Pacific slab, together with convective circulation process in the mantle wedge, led to mantle melting and the formation of intraplate volcanoes in NE China (Zhao, 2004; Lei and Zhao, 2005).

Our U–Th disequilibrium data, together with trace element data, can be used to evaluate the possible influence of subduction-related fluids in deep mantle. Uranium is highly mobile in oxidizing aqueous fluids whereas Th behaves as an immobile high field strength element. The subduction-related fluids are thus highly enriched in U relative to Th. Lavas formed by subduction-related fluid-induced melting often display ^{238}U excesses or U–Th equilibrium (Gill and Williams, 1990; Elliott et al., 1997; Bourdon et al., 2003; Turner et al., 2003), as well as high U/Th ratios (Fig. 7). The significant ^{230}Th excesses in the alkali basalts from Jingbohu and Long-gang argue against flux melting. The strongest evidence against fluid-induced melting comes from the Long-gang volcanoes. Long-gang is closer to the subduction trench compared with Wudalianchi and Jingbohu. The significant 33–35% ^{230}Th excesses in the Long-gang lavas are uncharacteristic of any subduction-related volcanism.

Although arc lavas with rare ^{230}Th enrichments have been observed from Nicaragua, central America (Reagan et al., 1994; Thomas et al., 2002), these arc lavas from Nicaragua are also characterized by very high (^{238}U/^{232}Th) ratios (1.4 to 2.8) (Fig. 7). In contrast, the (^{238}U/^{232}Th) ratios of the young lavas from NE China are 0.72 to 0.84 for Jingbohu and 0.60 to 0.62 for Long-gang (Table 2).

Table 2
U–Th disequilibrium and Nd, Sr and Pb isotopic compositions

Samples	J99821-5	J99821-1	J99822-1	J99823-1	J99824-1	JB11-11	LG9940	99L11-1	HJ97001A	P-2	P-4
Locations	Jingbohu	Jingbohu	Jingbohu	Jingbohu	Jingbohu	Jingbohu	Long-gang	Long-gang	Long-gang	Tianchi	Tianchi
U	1.93	1.76	2.62	1.93	1.98	2.45	1.25	1.70	1.12	8.89	2.25
Th	7.55	7.21	9.53	8.15	7.86	9.81	6.14	8.61	5.65	42.57	10.90
U/Th	0.256	0.244	0.275	0.237	0.252	0.250	0.204	0.197	0.198	0.209	0.206
(^{238}U/^{232}Th)	0.777	0.743	0.836	0.721	0.765	0.759	0.621	0.601	0.601	0.634	0.628
(^{230}Th/^{232}Th)	0.909	0.855	0.938	0.922	0.876	0.825	0.827	0.809	0.796	0.711	0.705
(^{230}Th/^{238}U)	1.17	1.15	1.12	1.28	1.15	1.09	1.33	1.35	1.33	1.12	1.12
^{87}Sr/^{86}Sr	0.704114		0.704409	0.703938			0.704467	0.704443	0.704488	0.705154	0.705020
2SE	0.000009		0.000006	0.000009			0.000009	0.000011	0.000011	0.000009	0.000015
^{143}Nd/^{144}Nd	0.512801		0.512713	0.512805			0.512665	0.512674	0.512663	0.512582	0.512586
2SE	0.000008		0.000008	0.000008			0.000008	0.000008	0.000008	0.000008	0.000009
εNd	3.2		1.5	3.3			0.5	0.7	0.5	−1.1	−1.0
^{208}Pb/^{204}Pb	37.958		38.044				38.394	38.480	38.457	37.934	37.897
^{207}Pb/^{204}Pb	15.505		15.508				15.570	15.556	15.546	15.541	15.532
^{206}Pb/^{204}Pb	18.000		17.876				17.910	17.953	17.931	17.560	17.540

$\varepsilon_{Nd} = [(^{143}Nd/^{144}Nd)/(^{143}Nd/^{144}Nd)_{CHUR} - 1] \times 1000$, where $(^{143}Nd/^{144}Nd)_{CHUR} = 0.512638$.

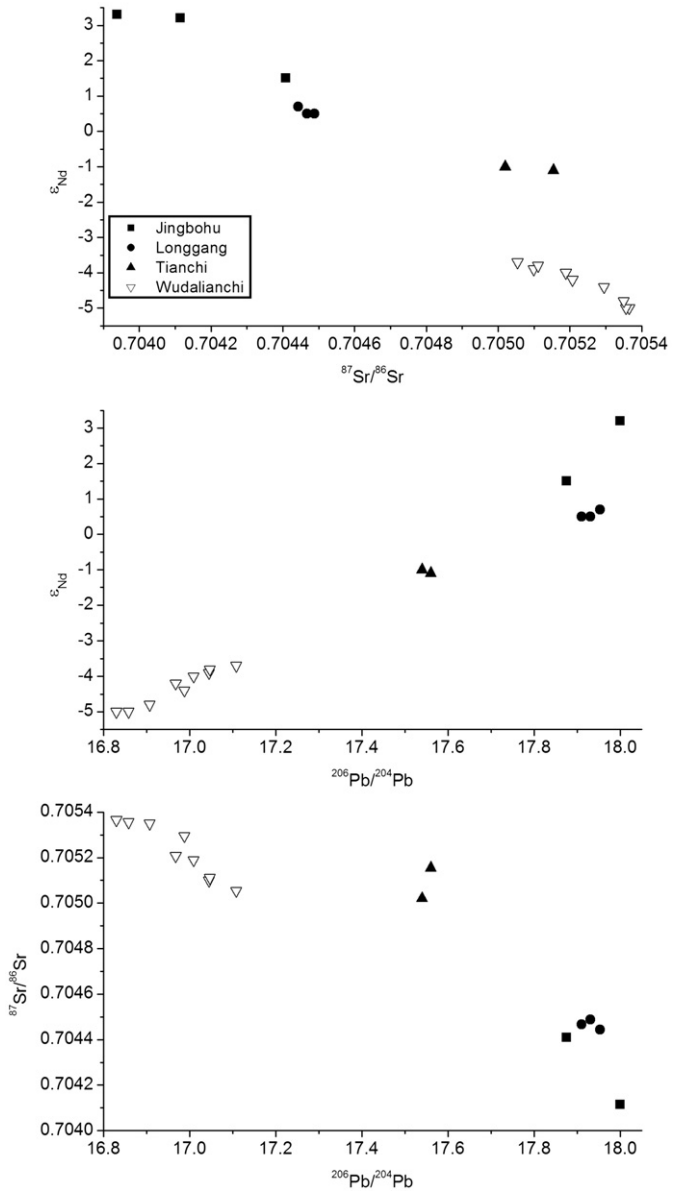

Fig. 5. Covariations in (a) ε_{Nd} vs. $^{87}Sr/^{86}Sr$, (b) ε_{Nd} vs. $^{206}Pb/^{204}Pb$, and (c) $^{87}Sr/^{86}Sr$–$^{206}Pb/^{204}Pb$ for the Holocene lavas from NE China.

Their U/Th ratios are even lower than the continental basalts from western USA (Fig. 6). Thus significant ^{230}Th excesses together with low U/Th ratios in the NE China volcanic rocks argue against the influence of the fluids released from the subducted Pacific slab.

In addition to U–Th disequilibrium data, we can assess the possible role of subduction-related fluids using trace element data. During the slab dehydration process, Ba and Sr are highly mobile in fluids from the subducted slab whereas Th is much less mobile. Thus fluid fluid-induced melting would produce lavas with high Ba/Th and Sr/Th ratios. With exception of several samples from Sunda, arc lavas produced by fluid-induced melting typically have Ba/Th ratio ranging from 130 to 970 (Bourdon et al., 2003) and Sr/Th ratios ranging from 187 to 1641 (Hawkesworth et al., 1997). The Jingbohu and Long-gang lavas exhibit rather low Ba/Th and Sr/Th ratios. The Ba/Th ratios range from 61 to 90 for the Jingbohu lavas, and from 91 to 135 for the Long-gang lavas. The Sr/Th ratios are 92–140 for Jingbohu and 75–133 for Long-gang (Fig. 8).

High field strength elements such as Nb and Ta behave similarly to the immobile Th during slab dehydration. The fluid-induced melting

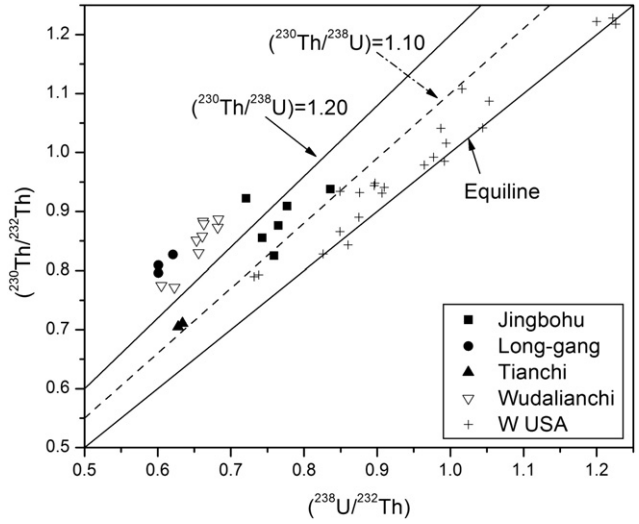

Fig. 6. U–Th disequilibrium data for Jingbohu, Long-gang and Tianchi lavas. The Wudalianchi U–Th isotope data are from Zou et al. (2003). The U–Th isotopes data for W USA Holocene basalts are from Asmerom and Edwards (1995) and Reid (1995).

thus can generate lavas with negative anomalies in Nb and Ta. Jingbohu and Long-gang alkali basalts display positive Nb and Ta anomalies (Fig. 4), which does not indicate the involvement of subduction-related fluids or sediments.

To sum up, the significant ^{230}Th excesses, low U/Th, Ba/Th and Sr/Th ratios, and the positive anomalies in Nb and Ta, consistently argue against the involvement of subduction-related fluids to generate the young volcanoes in NE China.

How far can Pacific subduction-related fluids go? The underlying mantle to generate the NE Japan alkali basalts was strongly affected by the fluids released from the subducting Pacific plate (Kimura and Yoshida, 2006). The alkaline basalts from NE Japan indeed display positive ^{238}U excesses (Yokoyama et al., 2003; Yokoyama et al., 2006), consistent with significant influence of subduction-related fluids. The underlying mantle to generate the SW Japanese alkali basalts was only slightly influenced by the subduction-related fluids. The alkaline basalts from SW Japan show reduced influence of subduction-related fluids. The intensity of the influence of subduction-related fluids thus

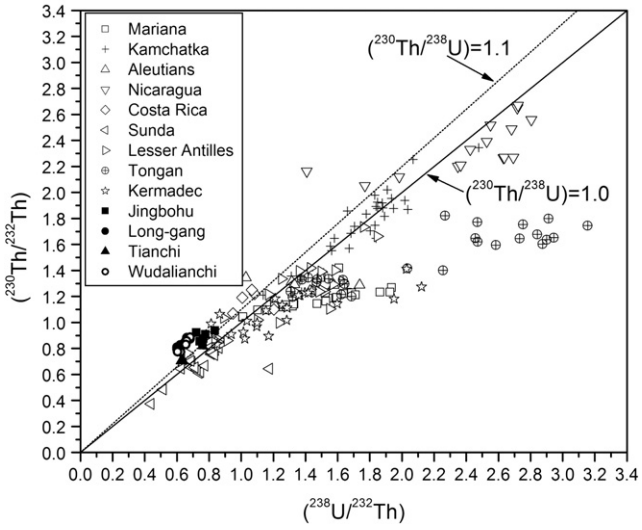

Fig. 7. Comparison of U–Th disequilibrium data of NE China young lavas with those of island arcs. Data sources for island arcs: Nicaragua (Reagan et al., 1994), Tongga-Kermadec (Turner et al., 1997), Mariana (Elliott et al., 1997), Kamchatka (Turner et al., 1998; Dosseto et al., 2003), Aleutians (Turner et al., 1998), Tonga (Turner et al., 1997), Costa Rica (Thomas et al., 2002) and Sunda (Turner and Foden, 2001).

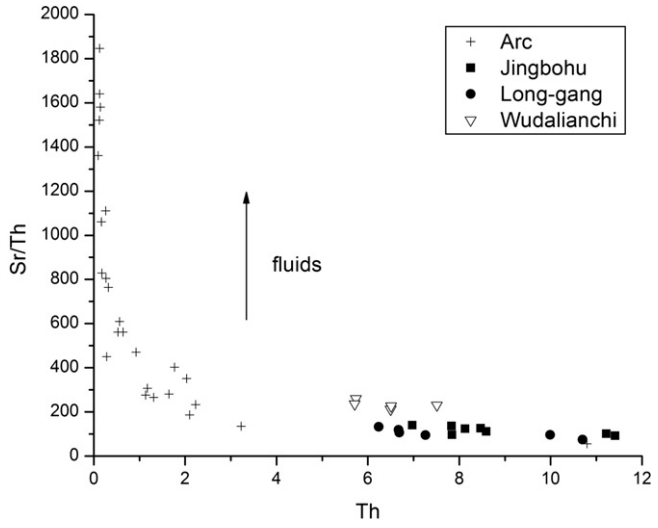

Fig. 8. Sr/Th vs. Th diagram. The Sr and Th concentration data of arc lavas are from Hawkesworth et al. (1997).

decreases with distance from the trench (Nakamura et al., 1985). The basalts from NE China do not show any influence of the subduction-related fluids. The distance from the young volcanoes of NE China to the Japan trench is about 1000 km, and subduction-related fluids thus may not go as far as 1000 km, although absence of evidence from young volcanoes is not always the evidence of absence of fluids in deep slab.

4.2. Melt generation mechanism

Melt can be generated by heating (temperature increase), decompression (pressure decrease) or the addition of fluids that reduced the mantle solidus temperature. If we can rule out the involvement of deep dehydration processes in the generation of the NE China lavas, then the remaining possibilities include (1) hot plume melting above the mantle solidus, and (2) decompression melting.

$^{3}He/^{4}He$ ratios are a useful tracer of mantle plume origin. Their low $^{3}He/^{4}He$ ratios, ranging from 5 to 7 times the atmospheric ratio (Chen et al., 2007), are not consistent with deep mantle plume origins (Chen et al., 2007). The dispersed nature of the volcanism does not support plume melting, either. Although dispersed volcanism preceded the Deccan Traps, the volume was significantly higher than NE China. In addition, recent seismic topographic images show that the seismic velocity anomalies beneath volcanic fields in NE China are shallow, and lack any deep roots that would indicate a deep-seated hotspot or mantle plume (Zhao et al., 2004). Furthermore, continental lavas generated by plume melting would reveal compositional trends of early lithospheric melts followed by asthenospheric magmas after the lithosphere has thinned (Turner et al., 1996; Rodgers et al., 2006). In contrast, the lithospheric melt with negative ε_{Nd} (− 3.7 to − 5.0) at Wudalianchi (Zou et al., 2003) is the youngest melt in the NE China. Thus there is no substantial evidence for the presence of a Cenozoic mantle plume beneath NE China.

If neither plume melting nor deep dehydration fluid-induced melting is the main mechanism to generate melt in NE China, then decompression melting might play the dominant role in the melt generation. The decompression melting of the upwelling asthenosphere may be related to the extensional stresses in back-arc regions (Nakamura and Uyeta, 1980) induced by rolling back of the Pacific Plate that started from Miocene (Ren et al., 2002).

We further postulate that, in addition to the convective circulation process in the mantle wedge induced by slab rolling back, the piling up and upward thickening of the dry and stagnant Pacific slab in the mantle transition zone may contribute to the asthenosphere upwelling far from the trench (Fig. 9). The thickness of the subducting Pacific slab beneath Japan is 80–90 km (Zhao et al., 1994; Deal and Nolet, 1999). In comparison, the thickness of the piling up stagnant slab underneath NE China is 150–200 km (Zhao, 2004). We speculate that the upward thickening of the piling up slab may help drive a broad asthenosphere upwelling underneath NE China far away from the trench. In this sense, the stagnant Pacific slab may have contributed forces, rather than materials (fluids), to the melt generation beneath NE China (Fig. 9). Clearly, the slab rolling back played important role in generating the melts above the mantle wedge not too far from the trench before the slab became flat. The basalts in the back-arc Japanese Sea may be generated by slab rolling back. In comparison, in places far from the trench where underneath slab already became flat and stagnant, the continuous slab piling up and upward thickening may play potentially important geodynamic role to the asthenosphere upwelling for the generation of young basalts in NE China.

4.3. Mantle upwelling rate

($^{230}Th/^{238}U$) in young basalts produced by decompression melting is sensitive to the rate of melting that is related to the solid mantle upwelling rate (McKenzie, 1985; Williams and Gill, 1989; Zou and Zindler, 2000). In the following, the Tianchi samples are excluded for the estimate of the mantle upwelling rate owing to their evolved feature in the magma chamber.

Two models have been proposed to quantify the extent of U–Th disequilibrium during decompression melting: (1) the dynamic melting model that was originally proposed by McKenzie (1985) and revisited by Williams and Gill (1989) and Zou and Zindler (2000), and (2) equilibrium percolation model (Spiegelman and Elliott, 1993; Lundstrom et al., 1995). Dynamic melting is a "zero-Damkohler number" channel flow model (melt–solid reaction is very slow relative to melt migration velocity) whereas the equilibrium percolation model is an "infinite Damkohler number" model (melt–solid reaction is very fast relative to melt migration velocity) (Sims et al., 1999; Zou, 2007). In all likelihood, reality lies somewhere in between the two end-member models and melt transport might be a fractal tree model (Hart, 1993). Recent Th–Ra and U–Pa disequilibrium data strongly support melt extraction via channels as the main mechanism of melt migration from the Earth's mantle (e.g., Bourdon et al., 2003; Stracke et al., 2006). In addition, since the equilibrium percolation model involves varying parameters, it is unlikely to invert these parameters from one measurement in ($^{230}Th/^{238}U$). We thus choose dynamic

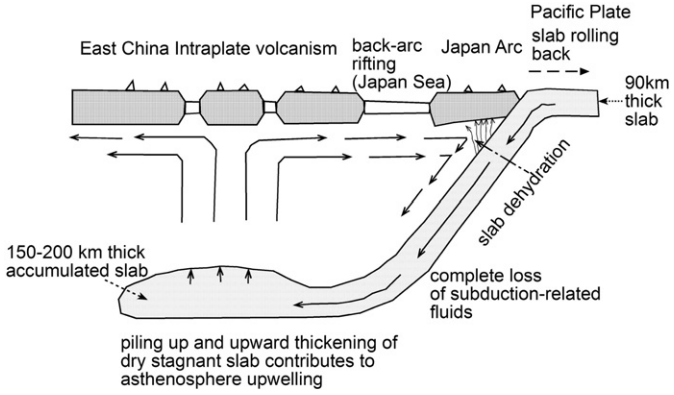

Fig. 9. Tectonic features of the NE Asia and NW Pacific (modified after Tatsumi et al. (1990) and Lei and Zhao (2005) to emphasize the accumulation and thickening of the stagnant slab). U-series data and trace element data argue against the deep dehydration process. We suggest that the piling up and thickening of the stagnant Pacific slab in the transition zone, together with the convective circulation process in the mantle wedge, help drive the asthenosphere upwelling and induce decompression melting.

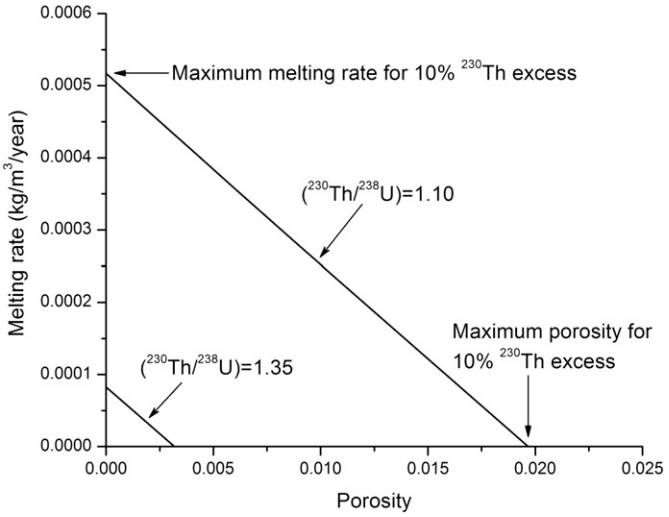

Fig. 10. Estimate of the maximum rate of mantle melting from U–Th disequilibrium data. Bulk partition coefficients are D_U=0.005 and D_{Th}=0.003 for garnet peridotites.

melting model for inversion by rewriting Eq. (30) in Zou and Zindler (2000) as

$$\dot{M}_{Max} = \frac{(\lambda_{238}+\lambda_{230})\lfloor \rho_f \phi + \rho_s(1-\phi)D_U \rfloor - Z\lambda_{230}\lfloor \rho_f \phi + \rho_s(1-\phi)D_{Th} \rfloor}{(Z-1)[1+\rho_f \phi/[\rho_s(1-\phi)]]} \quad (1)$$

where Z represents measured (^{230}Th/^{238}U) activity ratios, ϕ is the melting porosity, $\dot{M}$ is the melting rate, ρ_f and ρ_s represent the density of melt and solid, respectively. It should be emphasized that in the dynamic melting model, there is replenishment of materials to the melting column from below, and the melting rate is closely related to mantle upwelling rate and melt productivity. Because we have only one equation but two unknowns in $\dot{M}$ and ϕ, we cannot obtain unique solutions for $\dot{M}$ and ϕ but can, nevertheless, put some quantitative constraints on these variables. Melting rates and porosity in a garnet peridotite source that satisfy this relationship for a given value of (^{230}Th/^{238}U) are shown in Fig. 10. For melting rates to be non-negative, the melting porosity f must be < 2.0% for (^{230}Th/^{238}U) = 1.10, and < 0.3% for (^{230}Th/^{238}U) = 1.35. For non-negative values of ϕ, the melting rates $\dot{M}$ must be $< 5.2\times10^{-4}$ (kg/m^3/year) for (^{230}Th/^{238}U) = 1.10, and $<0.8\times10^{-4}$ (kg/m^3/year) for (^{230}Th/^{238}U) = 1.35 (Fig. 8). The melting rate can be used to estimate solid mantle upwelling velocity (W) in a one-dimensional melting column, by rewriting Eq. (17) in Spiegelman and Kenyon (1992) as

$$W = \frac{\dot{M}}{\rho_s(df/dz)} \quad (2)$$

where z (in km) represents the depth at a melting column. If the melt productivity $df/dz = 0.003$ km^{-1} is used (McKenzie and Bickle, 1988; Asimow et al., 1997), then the maximum solid mantle upwelling rate W_{Max} is < 5.2 cm/year for (^{230}Th/^{238}U) = 1.10, and < 0.8 cm/year for (^{230}Th/^{238}U) = 1.35.

If the solid mantle upwelling rates are similar in the NE China region, to satisfy the two constraints (W < 5.2 cm/year and W < 0.8 cm/year), then the smaller of the maximum rates is taken as the maximum upwelling rate for the region. We thus suggest that the mantle upwelling rate is < 0.8 cm/year. This indicates that the mantle upwelling caused by the accumulation and upward thickening of the stagnant slab is very slow in the NE China region.

4.4. Magma evolution time

U-series isotopic systematics in evolved magmas, such as trachyte and rhyolite, can be used to constrain the timescales of magma evolution (e.g., Bourdon et al., 1994; Hawkesworth et al., 2000; Condomines et al., 2003). Our U-series data of the Tianchi silicic rocks provide constraints on the time scale of magma evolution for Tianchi lavas from trachyte to rhyolite. Although these two samples erupted almost at the same time, the trachyte magma may have formed slightly earlier than the rhyolitic magmas in the magma chamber. The trachyte and rhyolite display different extent of fractional crystallization with SiO_2 = 64 and 71%, respectively. Their Eu anomalies are 0.21 for trachyte and 0.04 for rhyolite. But they have identical 12% ^{230}Th excesses. This indicates that the period of time required for the magma to change from 64% SiO_2 to 71% SiO_2 is smaller than the resolution of U–Th disequilibrium, which is about 10,000years (10ka).

For the three Long-gang basaltic samples (LG9940, 99L11-1, and HJ97001A) with U–Th isotope data, their SiO_2 contents vary from 47.5% to 50.4% and their MgO contents range from 7.4% to 4.5%. All three samples have essentially identical Nd, Sr and Nd isotopic compositions. Their similar 33–35% ^{230}Th excesses indicate that the magma evolution time required for the magma to change from 47.5% SiO_2 to 50.4% SiO_2 is also smaller than the resolution of the U–Th disequilibrium method (10ka).

After evaluating the magma evolution time within basaltic rocks from Long-gang, and the magma evolution time from trachyte to rhyolite from Tianchi, another question arises from the magma evolution time from basaltic magma to silicic magma (trachyte and rhyolite). If the silicic magma was derived from a basaltic magma, then the evolution time is:

$$\left(\frac{^{230}Th}{^{238}U}\right)_{silicic} = \frac{\lambda_{230}}{\lambda_{230}-\lambda_{238}}\left[1-e^{(\lambda_{238}-\lambda_{230})t}\right] + \left(\frac{^{230}Th}{^{238}U}\right)_{basalt} e^{(\lambda_{238}-\lambda_{230})t} \quad (3)$$

where $\lambda_{238} = 1.55125\times10^{-10}$year^{-1} and $\lambda_{230} = 9.156\times10^{-6}$year^{-1} (Cheng et al., 2000). The magma evolution time can be calculated by

$$t = \frac{1}{\lambda_{238}-\lambda_{230}} \ln \frac{\left(\frac{^{230}Th}{^{238}U}\right)_{silicic} - \frac{\lambda_{230}}{\lambda_{230}-\lambda_{238}}}{\left(\frac{^{230}Th}{^{238}U}\right)_{basalt} - \frac{\lambda_{230}}{\lambda_{230}-\lambda_{238}}}. \quad (4)$$

Since $\lambda_{238} \ll \lambda_{230}$, Eq. (4) can be simplified as

$$t = \frac{1}{\lambda} \ln \frac{\left(^{230}Th/^{238}U\right)_{basalt} - 1}{\left(^{230}Th/^{238}U\right)_{silicic} - 1} \quad (5)$$

The Long-gang basalts might be a more likely source for the Tianchi lavas as compared with the Jingbohu lavas. Long-gang is spatially closer to Tianchi, and both Long-gang and Tianchi belong to the greater Changbaishan volcanic field. In addition, the Long-gang lavas have (^{238}U/^{232}Th) ratios of 0.601–0.621, similar to Tianchi (0.628–0.634), whereas the Jingbohu lavas have much higher and variable (^{238}U/^{232}Th) (0.721–0.836) (Table 2). The ε_{Nd} values (+ 0.5 to + 0.7) of the Long-gang lavas are not very different from the Tianchi lavas (− 1.0 to − 1.1). The slight difference in ε_{Nd} values between the Long-gang and Tianchi lavas may reveal minor assimilation of the Tianchi lavas by crustal materials during fractional crystallization.

If we use (^{230}Th/^{238}U)$_0$ of 1.35 from Long-gang lavas as the starting magma and use (^{230}Th/^{238}U) of 1.12 for Tianchi trachytic magma, then the magma evolution time from basaltic magma to trachytic magma is calculated as 110ka. Note that assimilation of magma by older bulk crustal materials with (^{230}Th/^{238}U) of unity would reduce the extents of ^{230}Th excesses of the crystallizing Tianchi magmas. Thus the time interval of 110ka from basaltic magma to trachytic magma represents the maximum magma evolution time.

5. Conclusions

1. The small-volume Holocene volcanic rocks from Jingbohu, Long-gang, and Tianchi of NE China display positive ^{230}Th excesses (9 to 35%). Their ε_{Nd} values are + 1.5 to + 3.3 for Jingbohu lavas, + 0.5 to + 0.7 for the Long-gang lavas and − 1.1 to − 1.0 for the Tianchi lavas. All the volcanic rocks show positive Nb and Ta anomalies, low Ba/Th, Sr/Th and U/Th ratios. The chemical and isotopic compositions of the alkali basalts from Jingbohu and Long-gang indicate melting in the asthenospheric mantle.
2. The positive ^{230}Th excesses, positive Nb and Ta anomalies and low Sr/Th, Ba/Th and U/Th ratios of the alkali basalts from Jingbohu and Long-gang argue against chemical influence of the fluids released from the subducted Pacific slab. The small-volume volcanoes from NE China were not generated from the sediment melting or flux melting as a result of the subduction of the Pacific plate. The Pacific subduction may contribute the force for back-arc extension but did not directly contribute materials (metasomatic fluids). Such slab contribution is in the sense of physics rather than chemistry. The subduction-related fluids may have been lost before they could reach the mantle beneath NE China 1,000 km away from the trench.
3. The piling up and upward thickening of the stagnant subducted Pacific slab beneath NE China, together with the convective corner flow induced by slab rolling back, may provide the dynamic force to generate slow (0.8 cm/year) mantle upwelling far from the trench, leading to mantle decompression melting to form the young volcanoes at Jingbohu, Long-gang and Tianchi.
4. The magma evolution time form low SiO_2 (47.5%) basalt to higher SiO_2 (50.4%) basalt at Long-gang volcano is less than 10 thousand years. The magma evolution time from trachyte to rhyolite at Tianchi volcano is also less than 10ka. If the Tianchi silicic magmas were evolved from more primitive basaltic magmas similar to the Long-gang basalts, the magma evolution time from basaltic magma to silicic magmas is less than 110 thousand years.

Acknowledgements

Mark Reagan, Bernard Bourdon and an anonymous reviewer provided insightful and constructive reviews of the manuscript that significantly improved the quality of the manuscript. We are grateful to Axel Schmidt for his assistance with ion probe Th isotope measurement, and to Graham Layne for his generous advice regarding how to load chemically separated Th samples onto graphite disk. We are thankful to Xisheng Xu, Jianli Sui, and Qian Sun for their help with sample collection. One of us (HZ) thanks Kevin McKeegan, Mark Harrison and Mary Reid for support and mentoring, and Yang Chen for graphing advice. This work was funded by NSF (EAR 0711565) and NSF of China (40372044, 40125007). The ion probe facility was in part supported by the NSF EAR Instrumentation and Facility program.

References

Asimow, P.D., Hirschmann, M.M., Stolper, E.M., 1997. An analysis of variations in isentropic melt productivity. Phil. Trans. R. Soc. Lond. A 355, 255–281.

Asmerom, Y., Edwards, R.L., 1995. U-series isotope evidence for the origin of continental basalts. Earth Planet. Sci. Lett. 134, 1–7.

Ball, L., Sims, K.W.W., Weyer, S., Schwieters, J., 2002. Measurements of ^{232}Th/^{230}Th in volcanic rocks by PIMMS using the ThermoFinnigan Neptune. Geochim. Cosmochim. Acta Special Suppl. 2002 V. M. Goldschmidt Conference, 66, p. A47.

Basu, A.R., Wang, J.W., Huang, W.K., Xie, G.H., Tatsumoto, M., 1991. Major element, REE, and Pb, Nd and Sr isotopic geochemistry of Cenozoic volcanic rocks of eastern China: implications for their origin from suboceanic-type mantle reservoirs. Earth Planet. Sci. Lett. 105, 149–169.

Bourdon, B.P., 1994. Mass spectrometric measurements of U–Th disequilibrium in young volcanics: Implications for magmatic processes. Ph.D. thesis Thesis, Columbia Univ., New York.

Bourdon, B., Zindler, A., Worner, G., 1994. Evolution of the Laacher See magma chamber: evidence from SIMS and TIMS measurements of U–Th disequilibriua in minerals and glasses. Earth Planet. Sci. Lett. 126, 75–90.

Bourdon, B., Turner, S.P., Dosseto, A., 2003. Dehydration and partial melting in subduction zones: constraints from U-series disequilibria. J. Geophys. Res. 108 10.1029/2002JB001839.

Chen, Y., Zhang, Y.X., Graham, D., Su, S.G., Deng, J.F., 2007. Geochemistry Cenozoic basalts and mantle xenoliths in Northeast China. Lithos 96, 108–126.

Cheng, H., Edwards, R.L., Hoff, J., Gallup, C.D., Richards, D.A., Asmerom, Y., 2000. The half-lives of uranium-234 and thorium-230. Chem. Geol., 169, 17–33.

Choi, S.H., Mukasa, S.B., Kwon, S.T., Andronnikov, A.V., 2006. Sr, Nd, Pb and Hf isotopic compositions of late Cenozoic alkali basalts in South Korea: evidence for mixing between the two dominant asthenospheric mantle domains beneath East Asia. Chem. Geol. 232, 134–151.

Collerson, K.D., Palacz, Z., Turner, P.J., 1997. Precise measurement of U-series nuclides by high sensitivity magnetic sector multicollector ICP-MS. EOS 78 (46), F788.

Condomines, M., Gauthier, P.J., Sigmarsson, O., 2003. Timescales of magma chamber processes and dating of young volcanic rocks. In: Bourdon, B., Henderson, G.M., Lundstrom, C.C., Turner, S.P. (Eds.), Uranium-series Geochemistry. Reviews in Mineralogy and Geochemistry. Mineralogical Society of America.

Deal, M.M., Nolet, G., 1999. Slab temperature and thickness from seismic tomography 2. Izu-Bonin, Japan, and Kuril subduction zones. J. Geophys. Res. 104, 28802–28812.

Dosseto, A., Bourdon, B., Joron, J.L., Dupre, B., 2003. U–Th–Pa–Ra study of the Kamchatka arc: new constraints on the genesis of arc lavas. Geochim. Cosmochim. Acta 67, 2857–2877.

Dunlap, C.E., Gill, J.B., Palacz, Z.A., 1992. U/Th disequilibria in the large-volume chemically-zoned eruption of Baitoushan, 1010 AD. Eos, Trans. Am. Geophys. Union 73, 611.

Elliott, T., Plank, T., Zindler, A., White, W., Bourdon, B., 1997. Elemental transport from slab to volcanic front at the Mariana arc. J. Geophys. Res. 102, 14991–15019.

England, J.G., Zindler, A., Reisberg, L.C., Ruberstone, J.L., Salters, V., Marcantonio, F., Bourdon, B., Brueckner, H., Turner, P.J., Weaver, S., Read, P., 1992. The Lamont–Doherty-Geological-Observatory Isolab-54 isotope ratio mass spectrometer. Int. J. Mass Spectrom. Ion Process. 121, 201–240.

Fan, Q.C., Sui, J.L., Liu, R.X., Wei, H.Q., Li, D.M., Sun, Q., Li, N., 2002. Periods of Quarternary volcanic activity in Longgang area, Jilin province. Acta Petrologica Sinica 18, 495–500 (In Chinese with English abstract).

Fan, Q.C., Sun, Q., Li, N., Yin, J.H., Chen, H.Z., Gao, F., Zhang, C.J., 2003. The section of airfall clastic rock of Holocene volcano in Jingbohu region and its eruptive history. Seismol. Geol. 25, 3–11 (in Chinese with English abstract).

Fan, Q.C., Sun, Q., Li, N., Wang, T.H., 2006. Holocene volcanic rocks in Jingbo Lake region — diversity of magmatism. Prog. Nat. Sci. 16, 65–71 (in Chinese with English abstract).

Farmer, G.L., 2004. Continental basaltic rocks. In: Rudnick, R.L. (Ed.), The Crust. Treatise on Geochemistry. Elsevier, pp. 85–121.

Flower, M.F., Tamaki, K., Hoang, N., 1998. Mantle extrusion: a model for dispersed volcanism and DUPAL-like asthenosphere in East Asia and the West Pacific. In: Flower, M.F.J., Chung, S.L., Lo, C.H., Lee, T.Y. (Eds.), Mantle Dynamics and Plate Interaction in East Asia. Am. Geophys. Union, Washington, D. C., 67–88.

Gill, J.B., Williams, R.W., 1990. Th isotope and U-series studies of subduction-related volcanic rocks. Geochim. Cosmochim. Acta 54, 1427–1442.

Hart, S.R., 1993. Equilibration during mantle melting: a fractal tree model. Proc. Natl. Acad. Sci. 90, 11914–11918.

Hawkesworth, C.J., Turner, S.P., McDermott, F., Peate, D.W., van Calsteren, P., 1997. U–Th isotopes in arc magmas: implications for element transfer from the subducted crust. Science 276, 551–555.

Hawkesworth, C.J., Blake, S., Evans, P., Hughes, R., Mcadonald, R., Thomas, L.E., Turner, S.P., Zellmer, G., 2000. Time scales of crystal fractionation in magma chambers — integrating physical, isotopic and geochemical perspectives. J. Petrol. 41, 991–1006.

Horn, S., Schmincke, H.U., 2000. Volatile emission during the eruption of Baitoushan Volcano (China/North Korea) ca. 969 AD. Bull. Volcanol. 61, 537–555.

Irvine, T.N., Baragar, W.R.A., 1971. A guide to the chemical classification of the common volcanic rocks. Can. J. Earth Sci. 8, 523–548.

Kimura, J.I., Yoshida, T., 2006. Contributions of slab fluid, mantle wedge and crust to the origin of quaternary lavas in the NE Japan arc. J. Petrol. 47, 2185–2232.

Layne, G.D., Sims, K.W., 2000. Secondary ion mass spectrometry for the measurement of ^{232}Th/^{230}Th in volcanic rocks. Int. J. Mass Spectrom. 203, 187–198.

Le Bas, M.J., Le Maitre, R.W., Streckeisen, A., Zanettin, B., 1986. A chemical classification of volcanic rocks based on the total alkali–silica diagram. J. Petrol. 27, 745–750.

Lei, J.S., Zhao, D.P., 2005. P-wave tomography and origin of the Changbai intraplate volcano in Northeast Asia. Tectonophysics 397, 281–295.

Lundstrom, C.C., Gill, J., Williams, Q., Perfit, M.R., 1995. Mantle melting and basalt extraction by equilibrium porous flow. Science 270, 1958–1961.

McKenzie, D., 1985. 230Th–238U disequilibrium and the melting processes beneath ridge axes. Earth Planet. Sci. Lett. 72, 149–157.

McKenzie, D., Bickle, M.J., 1988. The volumn volume and composition of melt generated by extension of the lithosphere. J. Petrol. 29, 625–679.

Nakamura, E., Uyeta, S., 1980. Stress gradient in arc-back arc regions and plate subduction. J. Geophys. Res. 85, 6419–6428.

Nakamura, E., Campbell, I.H., Sun, S.S., 1985. The influence of subduction processes on the geochemistry of Japanese alkaline basalts. Nature 316, 55–58.

Pietruszka, A.J., Carlson, R.W., Hauri, E.H., 2002. Precise and accurate measurement of ^{226}Ra–^{230}Th–^{238}U disequilibria in volcanic rocks using plasma ionization multi-collector mass spectrometry. Chem. Geol. 188, 171–191.

Reagan, M.K., Morris, J.D., Herrstrom, E.A., Murrell, M.T., 1994. Uranium series and beryllium isotope evidence for an extended history of subduction modification of the mantle below Nicaragua. Geochim. Cosmochim. Acta 58, 4199–4212.

Reid, M.R., 1995. Processes of mantle enrichment and magmatic differentiation in the eastern Snake River Plain: Th isotope evidence. Earth Planet. Sci. Lett. 131, 239–254.

Ren, J.Y., Tamaki, K., Li, S.T., Zhang, J.X., 2002. Late Mesozoic and Cenozoic rifting and its dynamic setting in Eastern China and adjacent areas. Tectonophysics 344, 175–205.

Rodgers, N.W., Thomas, L.E., Macdonald, R., Hawkesworth, C.J., Mokadem, F., 2006. ^{238}U–^{230}Th disequilibrium in recent basalts and dynamic melting beneath the Kenya rift. Chem. Geol. 234, 148–168.

Sims, K.W.W., DePaolo, D.J., Murrell, M.T., Baldredge, W.S., Goldstein, S., Clague, D., Jull, M., 1999. Porosity of the melting zone and variations in the solid mantle upwelling rate beneath Hawaii: inferences from ^{238}U–^{230}Th–^{226}Ra and ^{235}U–^{231}Pa disequilibria. Geochim. Cosmochim. Acta 63, 4119–4138.

Spiegelman, M., Kenyon, P., 1992. The requirements for chemical disequilibrium during magma migration. Earth Planet. Sci. Lett. 109, 611–620.

Spiegelman, M., Elliott, T., 1993. Consequences of melt transport for uranium series disequilibrium in young lavas. Earth Planet. Sci. Lett. 118, 1–20.

Stracke, A., Zindler, A., Salters, V.J.M., McKenzie, D., Gronvold, K., 2003. The dynamics of melting beneath Theistareykir, northern Iceland. Geochem., Geophys., Geosys. 4, 8513. doi:10.1029/2002GC000347.

Stracke, A., Bourdon, B., McKenzie, D., 2006. Melt extraction in the Earth's mantle: constraints from U–Th–Pa–Ra studies in oceanic basalts. Earth Planet. Sci. Lett. 244, 97–112.

Sun, S.S., McDonough, W.F., 1989. Chemical and isotopic systematics of oceanic basalts: implications for mantle composition and processes. In: Saunders, A.D., Norry, M.J. (Eds.), Magmatism in the Ocean Basins. Geological Society Special Publication, London, pp. 313–345.

Tatsumi, Y., Maruyama, S., Nohda, S., 1990. Mechanism of backarc opening in the Japan Sea: role of asthenospheric injection. Tectonophysics 181, 299–306.

Thomas, R.B., Hirschmann, M.M., Cheng, H., Reagan, M.K., Edwards, R.L., 2002. (^{231}Pa/^{235}U)-(^{230}Th/^{238}U) of young mafic volcanic rocks from Nicaragua and Costa Rica and the influence of flux melting on U-series systematics of arc lavas. Geochim. Cosmochim. Acta 66, 4287–4309.

Todt, W., Cliff, R.A., Hanser, A., Hofmann, A.W., 1996. Evaluation of a ^{202}Pb–^{205}Pb double spike for high-precision lead isotope analysis. In: Basu, A.R., Hart, S.R. (Eds.), Earth processes: reading the isotopic code. Geophysical Monograph Am. Geophys. Union, pp. 429–437.

Turner, S., Foden, J., 2001. U, Th and Ra disequilibria, Sr, Nd and Pb isotope and trace element variations in Sunda arc lavas: predominance of a subducted sediment component. Contrib. Mineral. Petrol. 142, 43–57.

Turner, S., Hawkesworth, C., Gallagher, K., Stewart, K., Peate, D., Mantovani, M., 1996. Mantle plumes, flood basalts, and thermal models for melt generation beneath continents: assessment of a conductive heating model and application to the Parana. J. Geophys. Res. 101, 11503–11518.

Turner, S.P., Hawkesworth, C.J., Rogers, N.W., Bartlett, J., Worthington, T., Hergt, J., Pearce, J.A., Smith, I., 1997. ^{238}U–^{230}Th disequilibria, magma petrogenesis, and flux rates beneath the depleted Tonga-Kermadec island arc. Geochim. Cosmochim. Acta 61, 4855–4884.

Turner, S., McDermott, F., Hawkesworth, C., Kepezhinskas, P., 1998. A U-series study of lavas from Kamchatka and the Aleutians: constraints on source composition and melting processes. Contrib. Mineral. Petrol. 133, 217–234.

Turner, S.P., Bourdon, B., Gill, J.B., 2003. Insights into magma genesis at convergent margins from U-series isotopes. In: Bourdon, B., Henderson, G.M., Lundstrom, C.C., Turner, S.P. (Eds.), Uranium-series Geochemistry. Reviews in Mineralogy and Geochemistry, pp. 255–310.

Wei, H.Q., Wang, Y., Jin, J.Y., Gao, L., Yun, S.H., Jin, B.L., 2007. Timescale and evolution of the intracontinental Tianchi volcanic shield and ignimbrite-forming eruption, Changbaishan, Northeast China. Lithos 96, 315–324.

Williams, R.W., Gill, J.B., 1989. Effect of partial melting on the uranium decay series. Geochim. Cosmochim. Acta 53, 1607–1619.

Yokoyama, T., Kobayashi, K., Kuritani, T., Nakamura, E., 2003. Mantle metasomatism and rapid ascent of slab components beneath island arcs: evidence from ^{238}U–^{230}Th–^{226}Ra disequilibria of Miyakejima volcano, Izu arc, Japan. J. Geophys. Res. 108, 2329. doi:10.1029/2002/JB00213.

Yokoyama, T., Kuritani, T., Kobayashi, K., Nakamura, E., 2006. Geochemical evolution of a shallow magma plumbing system during the last 500years, Miyakejima volcano, Japan: constraints from ^{238}U–^{230}Th–^{226}Ra systematics. Geochim. Cosmochim. Acta 70, 2885–2901.

Zhao, D.P., 2004. Global tomographic images of mantle plumes and subducting slabs: insight into deep Earth dynamics. Phys. Earth Planet. Inter. 146, 3–34.

Zhao, D.P., Hasegawa, A., Kanamori, H., 1994. Deep structure of Japan subduction zone as derived from local, regional and teleseismic events. J. Geophys. Res. 99, 22313–22329.

Zhao, D.P., Lei, J.S., Tang, R.Y., 2004. Origin of the Changbai intraplate volcanism in Northeast China: evidence from seismic tomography. Chinese Sci. Bull. 49, 1401–1408.

Zou, H.B., 2007. Quantitative Geochemistry. Imperial College Press, Lonon, p. 287 pp.

Zou, H.B., Zindler, A., 2000. Theoretical studies of ^{238}U–^{230}Th–^{226}Ra and ^{231}Pa–^{235}U disequilibria in young lavas produced during mantle melting. Geochim. Cosmochim. Acta 64, 1809–1817.

Zou, H.B., Zindler, A., Xu, X.S., Qi, Q., 2000. Major and trace element, and Nd–Sr–Pb isotope studies of Cenozoic basalts in SE China: mantle sources, regional variations, and tectonic significance. Chem. Geol. 171, 33–47.

Zou, H.B., Zindler, A., Niu, Y., 2002. Constraints on melt movement beneath the East Pacific Rise from 230Th–238U disequilibrium. Science 295, 107–111.

Zou, H.B., Reid, M.R., Liu, Y.S., Yao, Y.P., Xu, X.S., Fan, Q.C., 2003. Constraints on the origin of historic potassic basalts from northeast China by U–Th disequilibrium data. Chem. Geol. 200, 189–201.